Experimental validation of regularized array element localization

Stan E. Dosso[a)]
School of Earth and Ocean Sciences, University of Victoria, Victoria, British Columbia V8W 3P6, Canada

Nicole E. B. Collison, Garry J. Heard, and Ronald I. Verrall
Defence Research and Development Canada (Atlantic), Dartmouth, Nova Scotia B2Y 3Z7, Canada

(Received 18 April 2003; revised 8 January 2004; accepted 5 February 2004)

This paper examines and validates regularized inversion for array element localization (AEL) by quantitative comparison of inversion results to direct measurements of receiver positions for a full-scale AEL survey. Regularized AEL treats both receiver and source positions as unknown parameters in a ray-based inversion; prior information on source/receiver positions, inter-receiver spacing in depth, and/or a smooth array shape can be included, subject to statistically fitting the acoustic data. Uncertainties in the recovered receiver positions are estimated via Monte Carlo appraisal. To study this approach, a specially stabilized, two-dimensional receiver array and a series of impulsive sources (imploding glass light bulbs) were deployed from shore-fast (motionless) Arctic sea ice. Sources and recordings were not synchronized in time, so AEL inversions are based on relative arrival times. Receiver positions were measured to an uncertainty of ~5 cm in each dimension [9 cm in three dimensions (3D)] using nonacoustic (optical) methods. Average AEL errors (difference between measured receiver positions and inversion results) of 13 cm in depth, 27 cm in the horizontal, and 30 cm in 3D, as well as good agreement between the measured errors and estimated AEL uncertainties validate the regularized approach and provide benchmarks for acoustic AEL. Receiver-position errors are quantitatively investigated as a function of the number of sources, source-position errors, and different regularizations. [DOI: 10.1121/1.1701897]

PACS numbers: 43.60.Pt, 43.30.Xm [WLS]

Pages: 2129–2137

I. INTRODUCTION

Advanced array processing methods, such as beamforming[1] and matched-field processing and inversion,[2–5] require accurate knowledge of the position of individual receivers in the array. For example, a general rule to achieve an array processing gain within 1 dB of the theoretical limit requires receiver positions be known within a tenth of a wavelength at the frequency of interest.[6,7] However, at-sea array deployment is not an exact procedure, and an acoustic survey is often required after deployment to localize the receivers, a procedure known as array element localization (AEL). AEL surveys typically consist of measuring the travel times of acoustic signals at the receivers from a number of sources positioned around the array. Given knowledge of the ocean sound-speed profile, the travel-time data can be inverted for estimates of the receiver positions. Simple surveys based on expendable impulsive sources (e.g., explosive charges or imploding glass light blubs[8,9]) without synchronization in time between source transmissions and the receiver recording system provide a practical approach to AEL that is widely used.[9–12]

Ideally, AEL inversion should address all (significant) sources of error in the acoustic survey, and incorporate available *a priori* information in addition to the measured data. For instance, although source positions are usually treated as known in AEL, in practice, errors in these positions are often significant and represent the limiting factor.[13–16] Regularized AEL[14] addresses this limitation by treating both source and receiver positions as unknown parameters (with prior estimates and uncertainties) in a ray-tracing based inversion. An unknown bias for the sound-speed profile is included to account for calibration errors in water-column measurements, and prior estimates of the inter-receiver spacing in depth can also be incorporated. For arrays that are expected to be essentially straight, a regularization can be formulated for the smoothest array shape subject to statistically fitting the acoustic data. This provides the simplest shape consistent with the data, with no deviations from a smooth array that are not resolved by the data (a common consequence of overfitting noisy data).[14] The uncertainties of the recovered receiver positions are estimated using nonlinear Monte Carlo appraisal.[14] Regularized AEL has been applied to fixed horizontal arrays,[14,17] moored vertical arrays,[17,18] towed arrays,[15,19] and freely drifting sonobuoy fields.[16] Note, however, that independent measurements of receiver positions were not available in any of these applications to validate the AEL results, nor does it appear that any such "ground-truthing" of AEL methods has been reported to date.

The goal of this paper is to examine and validate regularized AEL by quantitative comparison of inversion results to direct measurements of receiver positions for a full-scale AEL survey. High-precision nonacoustic measurement of receiver positions required novel approaches. The experiment was carried out from shore-fast Arctic sea ice, which pro-

a)Electronic mail: sdosso@uvic.ca

vided a motionless platform. The array consisted of a horizontal line array (HLA) of geophones on the ice surface and a vertical line array (VLA) of hydrophones below the ice. A special six-point suspension system was employed to constrain the VLA in three dimensions so that it did not move with currents during the experiment.[20,21] Receiver positions were measured using a laser survey for the HLA and a remotely operated vehicle (ROV) for the VLA. Light-bulb sources were deployed at a number of positions around the array. The regularized AEL results are compared to the measured receiver locations, and the resulting errors are compared to the uncertainties estimated using Monte Carlo appraisal. Several cases are examined to quantitatively investigate the effect of the number of sources, treatment of source-position errors, and different forms of *a priori* information (i.e., different regularizations). The results presented here represent an important benchmark for the accuracy of acoustic AEL surveys of this type.

II. REGULARIZED AEL INVERSION ALGORITHM

The theoretical background and implementation for regularized AEL inversion has been reported previously.[14,15] This section provides an updated overview of the approach with several new elements; more complete treatments of the general theory of regularized inversion can be found elsewhere.[22–24] For AEL inversion, the relative travel times from sources to receivers can be written in vector form as

$$\mathbf{t}=\mathbf{T}(\mathbf{m})+\mathbf{n}. \tag{1}$$

In Eq. (1), the model $\mathbf{m}$ of unknown parameters consists of the three-dimensional (3D) position (x,y,z) of each receiver, the 3D position and transmission instant of each source, and a bias correction term for the sound-speed profile. The forward mapping $\mathbf{T}(\mathbf{m})$ represents the acoustic travel times along ray paths from source to receiver, and contains all of the physics and geometry of the problem. Finally, $\mathbf{n}$ represents the data errors (noise), with the assumption that the error n_i on datum t_i is due to an independent, Gaussian-distributed random process with zero mean and standard deviation σ_i. The inverse problem of determining $\mathbf{m}$ from $\mathbf{t}$ is functionally nonlinear. However, a local linearization can be obtained by expanding $\mathbf{T}(\mathbf{m})=\mathbf{T}(\mathbf{m}_0+\delta\mathbf{m})$ in a Taylor series to first order about an arbitrary starting model $\mathbf{m}_0$. Rearranging terms, this expansion can be written

$$\mathbf{J}\mathbf{m}=\mathbf{t}-\mathbf{T}(\mathbf{m}_0)+\mathbf{J}\mathbf{m}_0\equiv\mathbf{d}, \tag{2}$$

where $\mathbf{d}$ represents modified data defined in terms of known quantities and $\mathbf{J}$ is the Jacobian matrix of partial derivatives (sensitivities) $J_{ij}=\partial T_i(\mathbf{m}_0)/\partial m_j$ (an efficient formulation for computing ray travel times and analytic derivatives, including direct, turning, and reflected paths, is given in Refs. 15 and 16). Equation (2) represents a linear inverse problem which can be solved for $\mathbf{m}$ as described in the following. Since nonlinear terms are neglected, the inversion must be repeated iteratively while monitoring for convergence (discussed in the following).

Treating both source and receiver positions as unknown leads to an ill-posed problem that is not amenable to a standard least-squares solution.[22] The method of regularized inversion[14,22–24] provides a powerful approach to ill-posed problems based on incorporating physical *a priori* information to define a well-posed problem. Other approaches, such as singular-value decomposition and Levenberg–Marquardt inversion, are also applicable and provide a mathematically stable solution, but without the physical relevance imposed by prior information (discussed for AEL in Ref. 14). For regularized AEL inversion, three different forms of prior information can be imposed by including three regularization terms together with the data misfit in an objective function ϕ to be minimized:

$$\phi=|\mathbf{G}(\mathbf{J}\mathbf{m}-\mathbf{d})|^2+\mu_1|\mathbf{H}_1(\mathbf{m}-\hat{\mathbf{m}}_1)|^2+\mu_2|\mathbf{H}_2(\mathbf{m}-\hat{\mathbf{m}}_2)|^2+\mu_3|\mathbf{H}_3(\mathbf{m}-\hat{\mathbf{m}}_3)|^2. \tag{3}$$

In Eq. (3), the first term represents the χ^2 data misfit for the linear problem (given Gaussian data errors), with $\mathbf{G}=\mathrm{diag}[1/\sigma_i]$, and the remaining terms represent regularizations. The variables μ_1, μ_2, and μ_3 represent trade-off parameters (Lagrange multipliers) which determine the relative importance of the misfit and prior information in the minimization.

The first regularization term in Eq. (3) can be used to apply prior estimates for the model parameters, which in AEL applications consist of approximate knowledge of source and/or receiver positions from the deployment procedure. In this case, $\hat{\mathbf{m}}_1$ contains the prior estimates and the regularization matrix $\mathbf{H}_1$ weights the estimates according to their uncertainties,

$$\mathbf{H}_1=\mathrm{diag}[1/u_j], \tag{4}$$

where u_j represents the standard deviation of an assumed Gaussian uncertainty distribution for jth parameter.

The second regularization term in Eq. (3) can be used to apply prior information about the one-dimensional (1D) separation between receivers along a coordinate axis, such as depth or horizontal offset [specifying two-dimensional (2D) or 3D separations involves nonlinear constraints which cannot be included in linearized inversion]. To accomplish this, $\hat{\mathbf{m}}_2$ contains the expected 1D offsets v_j of the array along a coordinate axis to receiver j. Regularization matrix $\mathbf{H}_2$ consists of a (nonsquare) piecewise bidiagonal matrix (i.e., there are breaks between rows corresponding to the x, y, and z coordinates) with nonzero entries on the jth row given by

$$\mathbf{H}_2=\mathrm{diag}\left[\frac{-1}{v_{j+1}-v_j},\frac{1}{v_{j+1}-v_j}\right]. \tag{5}$$

This matrix weights prior information for closely spaced receivers more strongly than for widely spaced receivers, and has not been applied previously in regularized AEL inversion.

The third regularization term can apply the *a priori* expectation that the array shape is well approximated by a smooth function (i.e., the array shape involves minimal curvature or changes in direction). This can be applied using $\hat{\mathbf{m}}_3=0$ and $\mathbf{H}_3$ consisting of a (piece-wise) tridiagonal matrix with nonzero entries on the jth row given by

$$\mathbf{H}_3=\mathrm{diag}\left[\frac{-1}{(w_{j+1}-w_j)^2},\frac{w_{j+2}-w_j}{(w_{j+2}-w_{j+1})(w_{j+1}-w_j)^2},\frac{-1}{(w_{j+2}-w_{j+1})(w_{j+1}-w_j)}\right], \tag{6}$$

where w_j represents the expected 3D offset along the array to receiver j. Each row of $\mathbf{H}_3$ in Eq. (6) represents a discrete approximation to the second derivative operator $\partial^2/\partial w^2$ (note that for arrays with equally spaced receivers this simplifies to $\mathbf{H}_3 \propto \mathrm{diag}[-1,2,-1]$ which has been used previously[14–16]). Hence, $|\mathbf{H}_3\mathbf{m}|^2$ provides a measure of the total curvature of the array, and the regularization produces the minimum-curvature or smoothest (simplest) shape consistent with the acoustic data. The minimum-curvature regularization can be applied in one, two, or three dimensions, as appropriate.

Minimizing objective function (3) with respect to $\mathbf{m}$ yields the solution

$$\begin{aligned}\mathbf{m}=&[\mathbf{J}^T\mathbf{G}^T\mathbf{G}\mathbf{J}+\mu_1\mathbf{H}_1^T\mathbf{H}_1+\mu_2\mathbf{H}_2^T\mathbf{H}_2\\&+\mu_3\mathbf{H}_3^T\mathbf{H}_3]^{-1}\cdot[\mathbf{J}^T\mathbf{G}^T\mathbf{G}\mathbf{d}+\mu_1\mathbf{H}_1^T\mathbf{H}_1\hat{\mathbf{m}}_1\\&+\mu_2\mathbf{H}_2^T\mathbf{H}_2\hat{\mathbf{m}}_2+\mu_3\mathbf{H}_3^T\mathbf{H}_3\hat{\mathbf{m}}_3].\end{aligned} \tag{7}$$

Note that the second and third regularization terms are optional, and can be omitted if the appropriate prior information is not available by setting μ_2 and/or μ_3 to zero.

Implementation of the AEL algorithm consists of an iterative application of the regularized inversion (7), initiated from a starting model coinciding with the prior parameter estimates. Convergence of the algorithm is based on two criteria. First, the measured data must be fit such that the χ^2 misfit achieves its expected value of $\langle\chi^2\rangle=N$ for N data.[24] Note that although Eq. (7) is derived based on the linearized inverse problem, convergence must be judged in terms of the nonlinear misfit

$$\chi^2=|\mathbf{G}(\mathbf{T}(\mathbf{m})-\mathbf{t})|^2. \tag{8}$$

Second, a stable solution must be obtained such that the root-mean-square change in receiver positions between iterations is small compared to the expected accuracy of the solution (<1 cm for the present application). A practical aspect of implementing the inversion involves assigning values to the trade-off parameters, μ_1, μ_2, and μ_3. An effective procedure for two regularization terms is described in Refs. 14–16; extension to three regularizations is straightforward.

Uncertainty estimates for the regularized AEL solution are obtained using nonlinear Monte Carlo appraisal.[14–17,24] The source and receiver positions determined via inversion of measured data are assumed to define the true positions for a synthetic AEL problem, and acoustic travel-time data are computed for these positions. Subsequently, a large number of independent inversions of the synthetic data are carried out, each with different random errors applied to the data and to the prior source/receiver position estimates. The errors are drawn from Gaussian distributions with standard deviations corresponding to the estimated uncertainties for the measured data and priors. Standard deviations about the true positions are computed from the ensemble of synthetic inversion results to provide parameter uncertainty estimates.

The above-mentioned Monte Carlo procedure can be used to estimate localization errors in both an absolute sense (relative to the fixed, geographic coordinate system) and in a relative sense (relative to array-based coordinates). For relative error estimates, the effects of rigid-body translations and rotations of the individual inversion estimates (relative to the true positions) must be removed prior to computing error statistics. Translations are removed by aligning the 3D centroid of the estimated sensor positions with that of the true positions. To minimize the effects of rotations between a set of N estimated sensor positions (x_i,y_i) and reference positions (X_i,Y_i), an optimal rotation can be computed as follows. Measuring angles with respect to the x axis, rotated estimated positions are defined

$$\tilde{x}_i=r_i\cos(\theta_i+\psi),\quad \tilde{y}_i=r_i\sin(\theta_i+\psi), \tag{9}$$

where $r_i=[x_i^2+y_i^2]^{1/2}$, $\theta_i=\tan^{-1}(y_i/x_i)$, and ψ is the rotation angle to be determined. The l_2 error norm between the rotated and reference positions is defined

$$E=\sum_{i=1}^{N}\{[r_i\cos(\theta_i+\psi)-X_i]^2+[r_i\sin(\theta_i+\psi)-Y_i]^2\}. \tag{10}$$

Setting $\partial E/\partial\psi=0$ to minimize the error leads (after some algebra) to

$$\psi=\tan^{-1}\left[\frac{\Sigma_{i=1}^{N}r_i(Y_i\cos\theta_i-X_i\sin\theta_i)}{\Sigma_{i=1}^{N}r_i(X_i\cos\theta_i-Y_i\sin\theta_i)}\right]. \tag{11}$$

Applying the rotation angle given in Eq. (11) to the estimated sensor positions, Eq. (9), produces the position estimates with minimal error due to rotation.

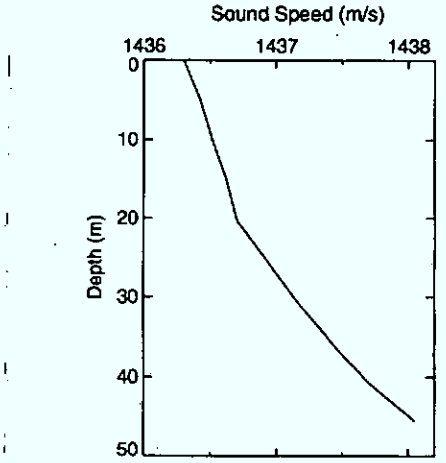

FIG. 1. Sound speed profile measured at experiment site.

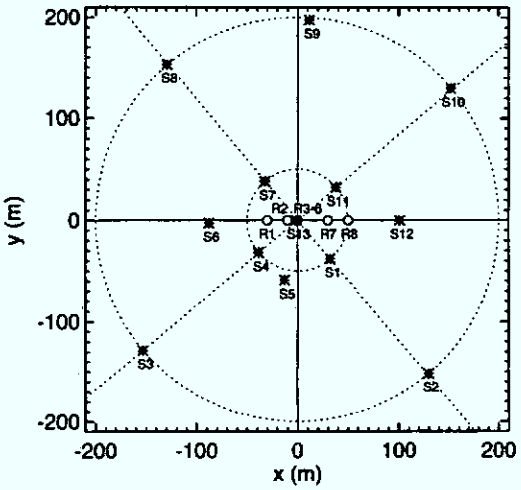

FIG. 2. Plan view of AEL survey. Open circles indicate receiver locations, with the VLA at the origin; asterisks indicate source positions.

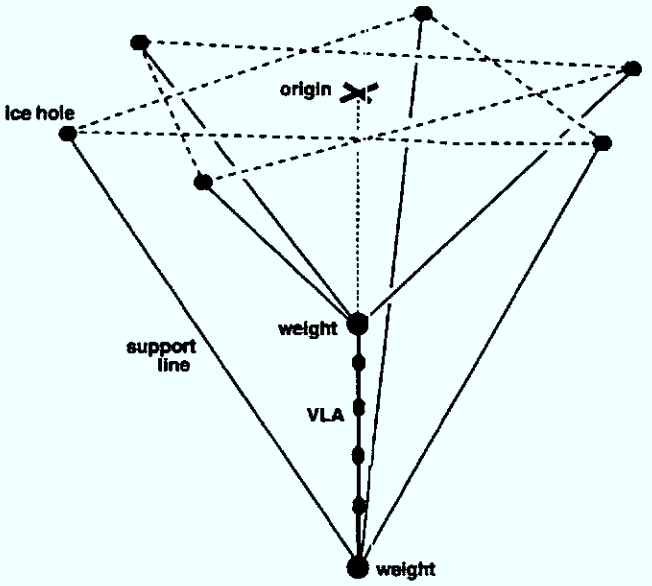

FIG. 3. Stable six-point suspension system used to prevent VLA movement. The triangular arrangement supporting each end of the VLA involves three ice holes at distances of 40, 40, and 65 m from the origin.

III. EXPERIMENT AND DATA

The goal of this work is to compare the results of regularized AEL to actual receiver positions for a full-scale AEL survey. This requires high-precision (nonacoustic) measurements of receiver positions and a means of constraining the receivers so they did not move during the survey. To accomplish this, the experiment was performed on shore-fast ice of the Lincoln Sea north of Ellesmere Island, Canada, which provided a stable, motionless platform. The experiment site was on a large expanse of annual ice which ranged in thickness from 1.4 to 1.7 m, with a water depth of ~45 m. The weather during the experiment was clear and cold (−30 to −40 °C) with no wind, conditions that typically result in minimal ambient noise due to ice-cracking[25] or pressure ridging events.[26] The ocean sound-speed profile was measured using a CTD (conductivity, temperature, depth) cast, and ice properties were determined using a hammer seismic survey.[27] The water-column sound speed, shown in Fig. 1, is upward-refracting over the entire 45 m depth, providing a clearly defined and unique direct ray path from source to receiver.

The receiver array consisted of an HLA of four vertical-component geophones on the ice and a VLA of four hydrophones suspended below the ice. The array is illustrated in plan view in Fig. 2 and receiver positions are given in Table I. The origin of the coordinate system for the experiment was taken to be directly above the intended position of the VLA, with the x axis aligned along the HLA and z defined to be positive downward from sea level. To ensure that the VLA receivers did not move with currents, a special suspension system was employed to constrain the VLA in three dimensions. This system supported each end of the VLA by three lines under tension in a triangular arrangement, as shown in Fig. 3. Weights of 16 and 28 kg were attached to the top and bottom of the VLA. This arrangement is comparable to supporting each end of the VLA by an inverted tripod, and a large lateral force is required to deflect the array by even a small amount (i.e., VLA deflections due to currents are assumed negligible). The potential difficulty is that there are in fact four lines supporting the bottom weight (three support lines and the VLA), and one of these could be slack. To counter this, an extensible member was included in series with the VLA. The spacing between the two ends of the VLA was adjusted so that the tension in the array was high enough to keep it straight, but not so high that the lower weight was lifted. An analysis of the stability of the suspension system is given in Refs. 20 and 21.

The positions of the HLA receivers were measured using a laser surveying instrument (geodimeter), which provided

TABLE I. Summary of receiver positions and their uncertainties from geodimeter and ROV measurements, and of measured AEL errors. Sensor type g/ph refers to a geophone and h/ph to a hydrophone.

Receiver	Sensor type	Measured positions (m)	Measurement uncertainties (cm)	AEL errors (cm)	
				Absolute	Relative
*R*1	g/ph	(−30.00,0.00,−0.15)	(5,5,5)	(10,61,6)	(30,5,9)
*R*2	g/ph	(−10.00,0.00,−0.15)	(5,5,5)	(43,86,15)	(24,11,10)
*R*3	h/ph	(0.33,0.13,31.75)	(7,7,5)	(36,53,31)	(17,18,26)
*R*4	h/ph	(0.32,0.12,32.75)	(7,7,5)	(35,56,12)	(15,12,12)
*R*5	h/ph	(0.31,0.12,33.26)	(7,7,5)	(35,54,11)	(16,10,16)
*R*6	h/ph	(0.18,0.03,38.67)	(7,7,5)	(42,47,40)	(23,13,17)
*R*7	g/ph	(30.00,0.00,−0.15)	(5,5,5)	(21,94,5)	(40,25,12)
*R*8	g/ph	(50.00,0.00,−0.15)	(5,5,5)	(9,99,7)	(25,12,9)

TABLE II. Summary of light-bulb source positions and uncertainties.

Source	Position (m)	Position uncertainties (m)
*S*1	(32.32,−38.14,40.00)	(1,1,0.5)
*S*2	(129.64,−152.22,40.00)	(1,1,0.5)
*S*3	(−153.36,−128.60,35.00)	(1,1,0.5)
*S*4	(−38.63,−32.10,40.00)	(1,1,0.5)
*S*5	(−12.95,−59.20,40.00)	(1,1,0.5)
*S*6	(−87.71,−2.68,40.00)	(1,1,0.5)
*S*7	(−32.27,38.22,40.00)	(1,1,0.5)
*S*8	(−129.42,153.06,40.00)	(1,1,0.5)
*S*9	(11.45,197.37,40.00)	(1,1,0.5)
*S*10	(152.01,129.49,40.00)	(1,1,0.5)
*S*11	(37.99,32.23,40.00)	(1,1,0.5)
*S*12	(101.00,0.00,40.00)	(1,1,0.5)
*S*13	(−1.50,0.00,10.00)	(0.5,0.5,0.25)

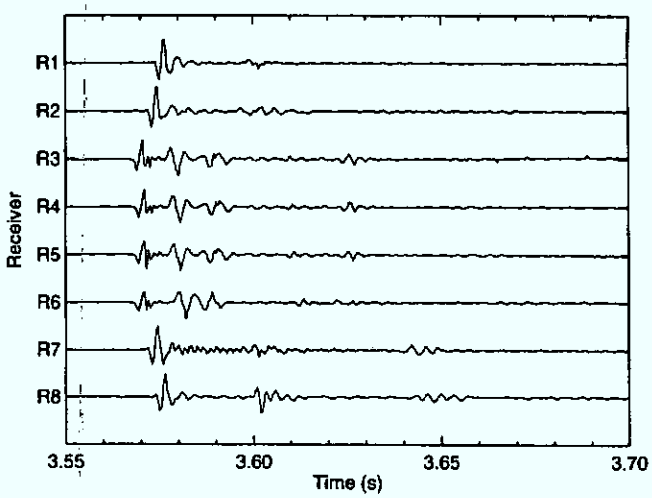

FIG. 4. Example of the recorded time series at the receiver array due to light-bulb source *S*9 in the AEL survey (time scale origin is arbitrary).

positioning accuracy to an estimated uncertainty of 5 cm. The positions of the VLA receivers were measured relative to a 5 kg lead ball lowered on a light kevlar line through the ice at the coordinate origin. The positions of the VLA hydrophones relative to the ball were estimated using the video display relayed from a ROV. The video indicated when the lead ball was aligned at the same depth as each hydrophone, providing depth measurements to an estimated uncertainty of 5 cm (this heavy ball on a light line will have negligible deflection due to currents). The horizontal positions of the hydrophones were estimated from the offset to the lead ball, using the ball's 10 cm diameter as a reference. This provided horizontal positions to within an estimated radial error of 10 cm. Assuming the radial error comprises equal, independent errors in x and y, an uncertainty of 7 cm was assigned to these coordinates. The receiver-position uncertainties are summarized in Table I.

The acoustic sources used for the AEL survey were glass light bulbs imploded under hydrostatic pressure in the water column.[8,9] To control the implosion depth, the light bulbs were attached to a 2 kg weight and lowered on a line through the ice to the desired depth; a messenger weight dropped along the line burst the bulb on impact. Three light-bulb sources were deployed at each of 13 positions around the receiver array, as shown in Fig. 2 and given in Table II. The source depths were 40 m at all but two sites. At source position *S*3 the water depth was less than 40 m, so the light bulbs were imploded at 35 m depth. Source position *S*13 was directly above the VLA, and, to avoid tangling lines, the light bulb was imploded at only 10 m depth. The positions of the source deployment holes were surveyed to high precision using the geodimeter; however, the actual position of the light bulbs at depth can vary due to currents in the water. The uncertainties in the measured source positions were estimated to be 1 m in x and y and 0.5 m in z for all sources except *S*13, where these uncertainties were halved due to the shallower deployment depth. Note that although the source position errors are treated as independent, there may be a systematic component due to currents deflecting all sources in the same direction. Systematic errors in source positions lead to a systematic errors in AEL receiver positions. However, such errors do not effect the relative receiver positions, which is the primary measure of AEL performance. The estimated source-position uncertainties are included in Table II. Note that it would be difficult to achieve the high-precision position measurements given in Tables I and II working in open waters.

Figure 4 shows an example of the recorded time series due to light-bulb source *S*9, digitized at a sampling rate of 2 kHz. The first strong impulsive arrival is clearly identified as the direct acoustic wave, with a well-defined first break and wave form indicative of a single arrival (i.e., uncomplicated by multipath, as expected given the simple form of the sound-speed profile in Fig. 1). The direct arrival is followed by a series of water-column multiples and general reverberation that decrease in amplitude with time. Note that the surface-reflected wave (phase-inverted arrival approximately 0.1 s after the direct arrival) is present at the VLA receivers ($R3-R6$), but not at the surface-mounted HLA receivers.

The data set used here for AEL consists of the direct arrival times averaged over the three recordings for each source position. Calculating this average required that the three sets of arrival times for each source position be optimally aligned in relative time, given that source instants are not known to provide an absolute time frame. This was accomplished using a grid search to determine the two time shifts that minimized an objective function consisting of the summation of the standard deviation about the mean over all arrivals.[14] Figure 5(a) shows the mean travel-time data for all sources and receivers. Since only relative travel times were measured, the data for each source are shown relative to the absolute travel time expected for receiver $R1$, as computed using ray-tracing and the measured positions for this receiver and all sources. Figure 5(b) shows the standard deviations about the mean. Most standard deviations are $\lesssim$0.2 ms; however, a small number are notably larger. In particular, the relatively large standard deviations obtained for source position *S*13 (directly above the VLA) are due to the shallow (10 m) source depth used here. Light-bulb implosions at shallow depths produce weaker acoustic signals with less high-frequency energy, resulting in poorly defined arrival times. These large errors are unfortunate, as source position *S*13

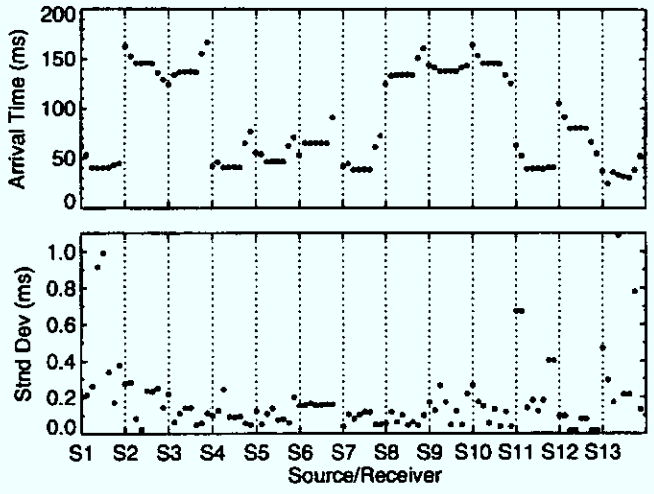

FIG. 5. Data collected in AEL survey: (a) mean arrival times and (b) standard deviations computed from three source deployments at each source location. Sources $S1-S13$ are identified on abscissa, and receivers are ordered $R1-R8$ for each source. The acoustic arrival could not be clearly identified for source $S6$, receiver $R8$ and is not included in the plot.

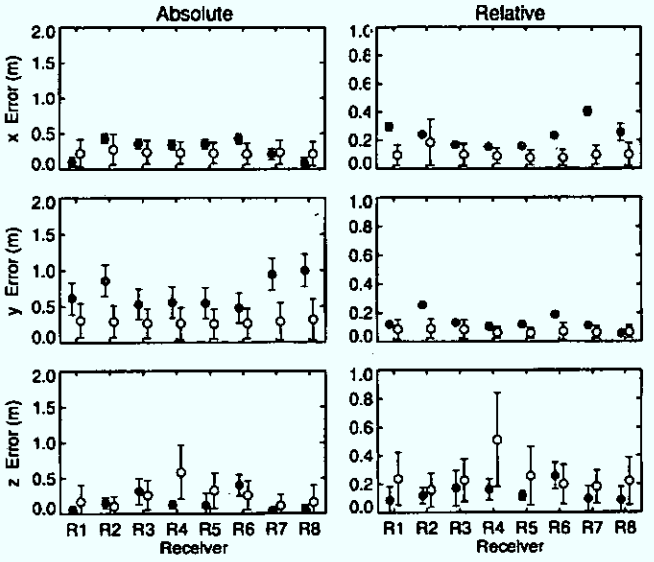

FIG. 6. Receiver localization errors from comparison with measured positions (closed circles) and Monte Carlo analysis (open circles) with prior source location uncertainties of 1 m in x and y and 0.5 m in z. The left column shows absolute errors; the right column shows relative errors.

provides important information constraining the VLA receiver depths. In practice, the small-scale fluctuations in the calculated standard deviations in Fig. 5(b) are not meaningful given the small sample size (three measurements). Hence, the standard deviations used in inversion were set to a fixed value of σ=0.2 ms for all data with standard deviations <0.3 ms. For data with standard deviations >0.3 ms, the actual standard-deviation values were used.

IV. RESULTS

This section applies the regularized algorithm developed in Sec. II to the AEL survey described in Sec. III, and compares the inversion results for receiver positions to the direct (nonacoustic) measurements. Several cases are considered to quantitatively study various aspects of the regularized inversion.

In the first case, travel-time data from all 13 sources (Fig. 2) are included in the inversion. The source positions were treated as unknown parameters, with starting and estimated values taken to be the measured values, and the source-position uncertainties (Table II) used to define the uncertainties in regularization matrix $\mathbf{H}_1$ of Eq. (4) for the source parameters. The minimum-curvature regularization is applied in x and y but not in z (since vertical smoothness is not physically meaningful for the VLA). To examine AEL results for receiver positions constrained primarily by the acoustic data, prior estimates for inter-receiving spacings are not applied in this case, but are considered subsequently. Also, to avoid using knowledge of the true receiver positions in the inversion, the starting values and prior estimates for the receiver positions were chosen at random from Gaussian distributions centered at the true parameter values with standard deviations of 50 m for x and y and 20 m for z. To obtain error measures that are independent of the starting values, the inversion was repeated 50 times, each time with a different set of random starting values/prior estimates for the receiver positions. Results are considered in terms of the mean error in x, y, z for each receiver (i.e., the absolute difference between the inversion results and the measured receiver positions, averaged over the 50 random initializations) and the standard deviation about these means. These measured errors are compared to the AEL uncertainties estimated from Monte Carlo appraisal with 50 random realizations.

Figure 6 shows the measured and estimated AEL errors, with one standard-deviation error bar included on each. The left column of Fig. 6 shows the inversion results in terms of absolute position errors, i.e., the errors relative to the fixed (geographical) coordinate system. However, for most array processing applications, the relative position errors (i.e., errors in an array-based coordinate system) are a more relevant measure of uncertainty. This is because position errors common to all receivers are equivalent to a simple translation and/or rotation of the receiver array, while relative position errors introduce inter-receiver timing and phase errors which can degrade or preclude some applications such as source localization or environmental inversion. The right column of Fig. 6 shows the AEL results in terms of relative positioning errors, computed as described in Sec. II. The measured errors (absolute and relative) for the receiver positions are also given in Table I.

Figure 6 shows that the Monte Carlo error estimates are similar to, but usually somewhat smaller than, the measured errors. The relative position errors are generally smaller than the absolute errors and have smaller variability. The measured relative errors averaged over all receivers are 13 cm in the vertical, 27 cm in the horizontal (i.e., 2D errors consisting of the square root of sum of squares of x and y errors), and 30 cm in 3D (the actual AEL errors are likely even smaller, since the measured receiver positions are themselves uncertain by 5–7 cm). These results indicate that regularized AEL inversion with imprecise source positions can provide highly accurate receiver positions, and that meaningful uncertainty estimates are provided by Monte Carlo appraisal. It is interesting to note that the 2D horizontal position errors are somewhat smaller for the VLA receivers ($R3-R6$), with

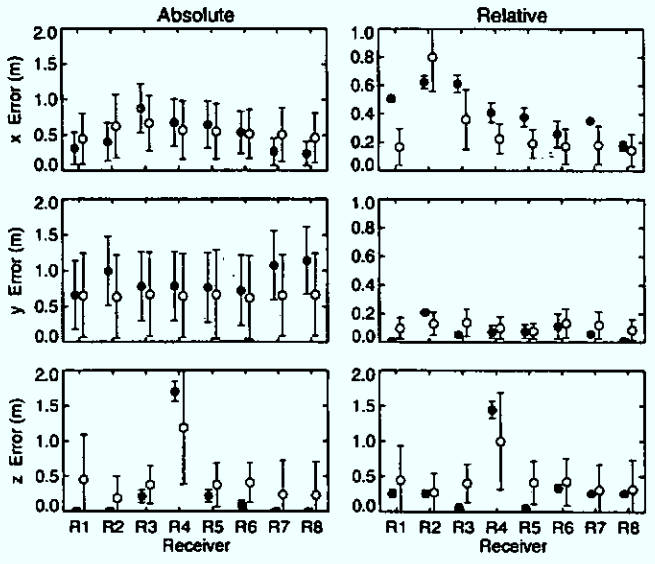

FIG. 7. Receiver localization errors from comparison with measured positions (closed circles) and Monte Carlo analysis (open circles) using data from only five sources, with prior source location uncertainties of 1 m in x and y and 0.5 m in z.

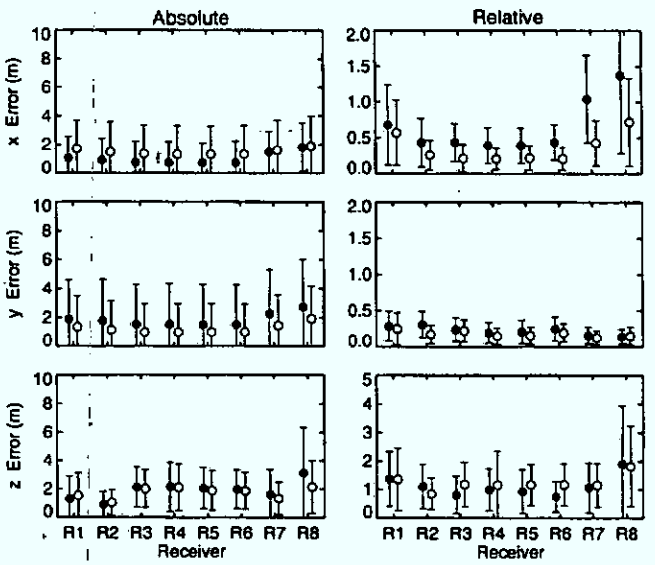

FIG. 8. Receiver localization errors from comparison with measured positions (closed circles) and Monte Carlo analysis (open circles) with prior source location uncertainties of 30 m in x and y and 4 m in z.

an average relative error of 22 cm. This is likely because the distribution of the close-range sources is centered on the VLA (Fig. 2), providing superior horizontal control. Further, the x component of the relative errors is generally larger than the y errors in all cases considered in this paper, likely because since the array is aligned along the x axis, the rotation correction has little effect on these errors (but a significant effect on y errors). Finally, in all inversion results in this paper, the sound-speed bias was found to be negligibly small (~0.1 m/s).

The AEL inversion results in Fig. 6 made use of all 13 source positions. To investigate the dependence on the number of sources, Fig. 7 shows inversion results computed for an identical problem, except that only five sources were employed: $S2$, $S3$, $S8$, $S9$, and $S13$ (see Fig. 2). Figure 7 shows that good localization results are still obtained, although the mean positioning errors and variability are generally somewhat larger for the smaller number of sources (cf. Fig. 6). The large positioning error in z for VLA receiver $R4$ is due to the large uncertainty associated with the arrival time for the shallow source $S13$ (directly above), as shown in Fig. 5. This error is larger in Fig. 7 than in Fig. 6 since no other short-range sources were included which provide strong vertical-positioning information.

In most at-sea AEL surveys, the uncertainties in source positions are larger than those obtained here for the through-the-ice survey. To consider such cases, random errors were added to the source positions used in the inversion of the measured AEL data (all 13 sources are included here). These errors were drawn from zero-mean Gaussian distributions with standard deviations of 30 m for x and y, and 4 m for z (representative of uncertainties due to GPS positioning and oceanic swells). Similar source-position errors were included in the Monte Carlo appraisal. The results of the AEL inversion with increased source-position errors, shown in Fig. 8, are significantly poorer than those in Fig. 6. However, useful receiver positions are still obtained. The measured relative (2D) horizontal errors are typically are $\lesssim$1 m, with errors of 20–40 cm for the receivers near the center of the source distribution ($R2$–$R6$). The relative errors in z vary from approximately 1 to 2 m. One way to improve AEL results is to include additional *a priori* information (if available). As an example, Fig. 9 shows AEL results for a case identical to that of Fig. 8, except that prior information of the vertical inter-receiver spacing was included. Figure 9 show a substantial improvement in receiver positions in all three dimensions, with measured relative errors $\lesssim$10 cm in z and 10–60 cm in the horizontal.

To quantify the benefit of including the source positions as unknown parameters in the regularized inversion, Fig. 10 shows AEL results for a case identical to that of Fig. 8 (i.e., 13 sources with large position errors), except that the inac-

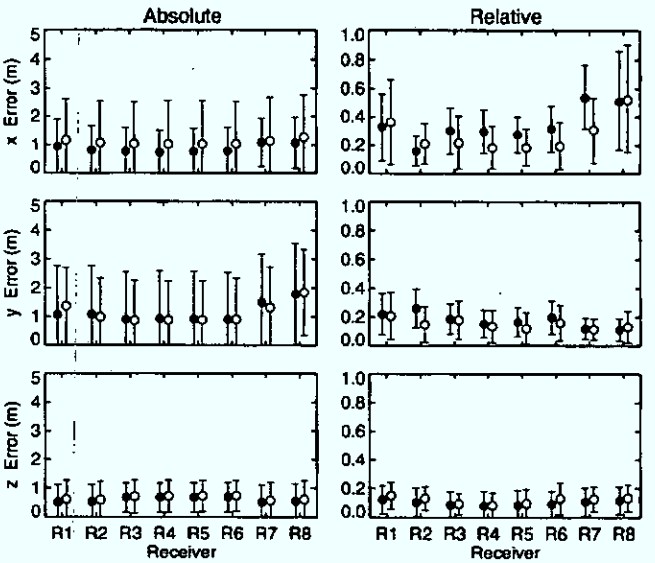

FIG. 9. Receiver localization errors from comparison with measured positions (closed circles) and Monte Carlo analysis (open circles) with prior source location uncertainties of 30 m in x and y and 4 m in z and prior information on vertical sensor spacing.

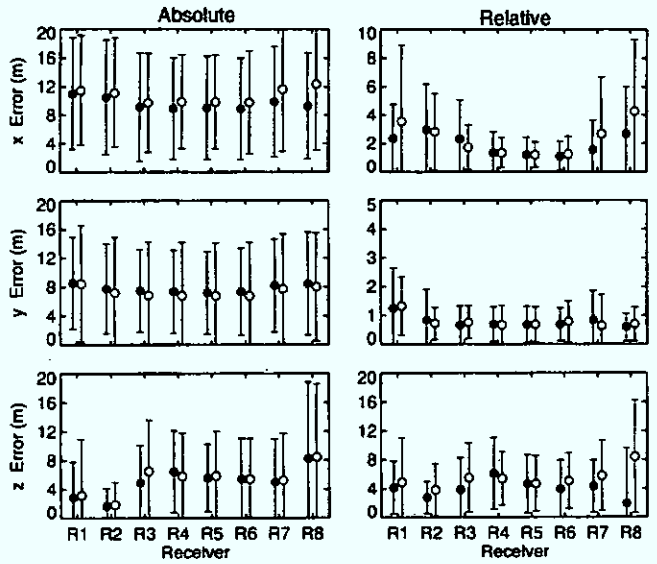

FIG. 10. Receiver localization errors from comparison with measured positions (closed circles) and Monte Carlo analysis (open circles) with prior source location uncertainties of 30 m in x and y and 4 m in z when source locations are not included in the AEL inversion.

curate source positions were held fixed, as is often done in AEL. The results in Fig. 10 are substantially worse than those in Fig. 8, with measured relative errors of 1–3 m in x and y and 2–6 m in z. Even poorer results would be expected for fewer sources. Finally, it should be noted that Figs. 6–10 all show good general agreement between the measured receiver-position errors and the Monte Carlo uncertainty estimates.

V. SUMMARY AND DISCUSSION

Array element localization is an important prerequisite for advanced array processing, but little work has been reported to date that quantitatively examines the accuracy of AEL results. This paper considered the method of regularized AEL by comparing inversion results to direct measurements of receiver positions for a full-scale AEL survey. To achieve this, a stabilized 2D array was deployed from shorefast (motionless) sea ice. Receiver positions were measured to ~5 cm accuracy in each dimension (9 cm in 3D) using nonacoustic methods (laser survey, ROV video). Impulsive sources were deployed around the array, with source positions known to ~1 m. The average measured AEL errors (difference between measured receiver positions and inversion results) were 13 cm in depth, 27 cm in the horizontal, and 30 cm in 3D. Generally good agreement was achieved between the measured errors and AEL uncertainties estimated by Monte Carlo appraisal. These results provide direct validation of the regularized AEL inversion methodology and its underlying assumptions (e.g., Gaussian-distributed data and prior-estimate uncertainties), and represent an important benchmark for acoustic AEL methods.

The effect on receiver-position errors of the number of sources included in the inversion and of the uncertainty in source positions was quantitatively investigated. Good AEL results were obtained with just five sources (four is the minimum possible for AEL with relative travel times). However, AEL results degraded significantly with increasing source-position uncertainties. A substantial increase in receiver-position errors occurred when source positions were not treated as unknown parameters in the inversion, indicating this is an important component of AEL inversion.

The results of this study indicate that even higher precision AEL results could be achieved by more tightly constraining source positions or by including prior information on inter-receiver spacings (if reliable information is available). Higher-precision results can also be obtained by inverting absolute travel-time measurements.[17,18] However, this requires synchronization in time between source transmissions and the recording system, resulting in a more complex AEL survey.

[1] W. S. Burdic, *Underwater Acoustic System Analysis* (Prentice-Hall, Englewood Cliffs, NJ, 1994).
[2] A. Tolstoy, *Matched Field Processing for Underwater Sound* (World Scientific, Singapore, 1993).
[3] A. B. Baggeroer, W. A. Kuperman, and P. N. Mikhalevsky, "An overview of matched field methods in ocean acoustics," IEEE J. Ocean. Eng. **18**, 401–424 (1993).
[4] M. D. Collins, W. A. Kuperman, and H. Schmidt, "Nonlinear inversion for ocean-bottom properties," J. Acoust. Soc. Am. **92**, 2770–2783 (1992).
[5] S. E. Dosso, M. L. Yeremy, J. M. Ozard, and N. R. Chapman, "Estimation of ocean-bottom properties by matched-field inversion of acoustic field data," IEEE J. Ocean. Eng. **18**, 232–239 (1993).
[6] B. D. Steinberg, *Principles of Aperture and Array Systems Design* (Wiley, New York, 1976).
[7] W. S. Hodgkiss, D. E. Ensberg, J. J. Murray, G. L. D'Spain, N. O. Booth, and P. W. Schey, "Direct measurement and matched-field approaches to array shape estimation," IEEE J. Ocean. Eng. **21**, 393–401 (1996).
[8] G. J. Heard, M. McDonald, N. R. Chapman, and L. Jaschke, "Underwater light bulb implosions: A useful acoustic source," Proceedings MTS/IEEE Oceans 97, 1997, Vol. 2, pp. 755–762.
[9] T. C. Yang and C. W. Votaw, "Under ice reflections at frequencies below 1 kHz," J. Acoust. Soc. Am. **70**, 841–851 (1981).
[10] E. C. van Ballegooijen, G. W. M. van Mierlo, C. van Schoonveld, P. M. van der Zalm, A. T. Parsons, and N. H. Field, "Measurement of toward array position, shape, and attitude," IEEE J. Ocean. Eng. **14**, 375–383 (1989).
[11] R. C. Shockley, J. A. Rice, and P. Hursky, "Element localization for bottomed arrays without transponders," J. Acoust. Soc. Am. **95**, 2809 (1994).
[12] M. V. Greening, "Array element localization of rapidly deployable systems," Can. Acoust. **28**, 7–13 (2000).
[13] K. C. Creager and L. M. Dorman, "Location of instruments on the seafloor by joint adjustment of instrument and ship positions," J. Geophys. Res. B **87**, 8379–8388 (1982).
[14] S. E. Dosso, M. R. Fallat, B. J. Sotirin, and J. L. Newton, "Array element localization for horizontal arrays via Occam's inversion," J. Acoust. Soc. Am. **104**, 846–859 (1998).
[15] S. E. Dosso and N. E. Collison, "Regularized inversion for towed-array shape estimation," *Inverse Problems in Underwater Acoustics*, edited by M. Taroudakis and G. Makrakis (Springer, Berlin, 2001).
[16] S. E. Dosso and N. E. B. Collison, "Acoustic tracking of a freely drifting sonobuoy field," J. Acoust. Soc. Am. **111**, 2166–2177 (2002).
[17] S. E. Dosso and B. J. Sotirin, "Optimal array element localization," J. Acoust. Soc. Am. **106**, 3445–3459 (2000).
[18] S. E. Dosso, G. H. Brooke, S. J. Kilistoff, B. J. Sotirin, V. K. McDonald, M. R. Fallat, and N. E. Collison, "High-precision array element localization of vertical line arrays in the Arctic Ocean," IEEE J. Ocean. Eng. **23**, 365–379 (1998).
[19] S. E. Dosso and M. Riedel, "Array element localization for towed marine seismic arrays," J. Acoust. Soc. Am. **110**, 955–966 (2001).
[20] R. I. Verrall, "Tetrahedral underwater arrays and the effect of current on their shape," DREA Tech. Memo. 2000-093, 2000, 16 pp.
[21] R. I. Verrall and G. J. Heard, "Technique for the accurate positioning of objects in an ice-covered ocean," DREA Tech. Memo. 2000-103, 2000, 25 pp.

[22] W. Menke, *Geophysical Data Analysis: Discrete Inverse Theory* (Academic, Orlando, 1984).
[23] C. van Schooneveld, "Inverse problems: A tutorial survey," in *Underwater Acoustic Data Processing*, edited by Y. T. Chan (Kluwer, Dordrecht, 1989), pp. 393–411.
[24] W. H., Press, S. A. Teukolsky, W. T. Vetterling, and B. P. Flannery, *Numerical Recipes in Fortran*, 2nd ed. (Cambridge University Press, Cambridge, 1992).
[25] M. V. Greening and P. Zakarauskas, "Spatial and source level distributions of ice cracking in the Arctic Ocean," J. Acoust. Soc. Am. **95**, 783–790 (1994).
[26] M. V. Greening and P. Zakarauskas, "Pressure ridging spectrum level and a proposed origin of the infrasonic peak in Arctic ambient noise spectra," J. Acoust. Soc. Am. **95**, 791–797 (1994).
[27] S. E. Dosso, G. J. Heard, and M. Vinnins, "Source bearing estimation in the Arctic using ice-mounted geophones," J. Acoust. Soc. Am. **112**, 1390–1398 (2002).